

OXYGEN-ENHANCED HIGH TEMPERATURE LAMINAR FLAMES

Zhongxian Cheng,* Joseph A. Wehrmeyer,† Robert W. Pitz‡
Mechanical Engineering Department, Vanderbilt University, Nashville, TN 37235

Abstract

Planar oxygen-enhanced methane counterflow flames are investigated by optical diagnostics and numerical simulation. The major species concentrations and temperature measured from Raman scattering are compared to the detailed simulations of the flame formed between two opposed jets. The effect of stretch and the influence of oxygen concentration in the oxidizer on the flame structure are studied for nitrogen-diluted methane fuel (20% CH₄ in N₂). The oxygen concentration of reactants changes the flame temperatures dramatically. At the same stretch rate ($\kappa=60 \text{ s}^{-1}$), there is about 800 K difference in flame temperature when the oxidizer varies from 23% O₂ to 100% O₂. Simulations with the GRI-Mech 3.0 chemical kinetic mechanism show that model-data comparisons for reactants, products such as H₂O, and temperature agree very well. However, the measured CO₂ is consistently lower than the simulated results. This deviation becomes worse when the oxygen concentration increased. The measured oxygen levels are higher than predictions at the flame front where the predictions show the oxygen is consumed. The measured oxygen leaks through the flame zone at the various oxygen-enhanced levels except in the pure oxygen case where oxygen is completely consumed at the flame front. The measured extinction limit for the minimum of amount of fuel in the diluted fuel mixture is very close to the calculated result when pure oxygen is the oxidizer. But when air is the oxidizer, the measured extinction limit for the minimum fuel in the diluted fuel mixture (28% CH₄ in N₂) is very different from the calculated value (19% CH₄ in N₂). Both GRI-Mech 3.0 and Williams chemical kinetic mechanisms are used. At low-level enrichment (i.e., 30% O₂) and high level enrichment (100% O₂), GRI-Mech 3.0 and Williams mechanisms give almost identical predicted results.

Introduction

Oxygen-enhanced combustion had been used increasingly in industry over the last two decades to

improve productivity and reduce emissions.^{1,2} Unlike traditional combustion that uses air (21% O₂ by volume) as an oxidizer, oxygen-enhanced combustion has oxygen concentration varying from 21% to 100%. When 100% O₂ is used as the oxidizer, it is termed as an oxy/fuel flame. The fundamental effects of oxygen-enrichment on flame characteristics are high flame temperature, high flame speed, reduced flame length and increased flammability range.^{1,2} Increased efficiencies from burning fuel with pure O₂ instead of air can reduce CO₂ emissions and help alleviate global warming. Theoretically NO_x can be completely eliminated by oxy/fuel combustion. Unfortunately a small percentage of N₂ always exists in the fuel or oxidizer and NO_x emissions can be worse because of thermal NO_x formation at high temperature in the oxygen-enhanced flames.³ The effect of oxygen-enhancement on NO_x and soot formation has been widely investigated in counterflow flame studies.³⁻⁹ In industry, strategies are being proposed to reduce primary NO_x.¹⁰ Recently Qin and co-workers¹¹ have studied the effect of O₂ composition modulation on the dynamics and structure of lean CH₄/air premixed flames in light of its relevance to oxygen enhanced combustion in the stagnation flow configuration. They found that the addition of extra O₂ in the oxidizer noticeably extends the lean flammability limit and thus stable combustion can be achieved at leaner conditions, which are also characterized by reduced fuel consumption, lower flame temperatures and reduced NO_x emissions. NO formation during oxy/fuel combustion was studied with a counterflow burner by Sung and Law,³ where pathway and sensitivity analysis were used to identify key reactions contributing to the production of NO in oxy/fuel combustion and thermal NO was found to dominate.

In oxygen-enriched flames, high flame temperature, strong flame emissions and laser-induced fluorescence (LIF) interference has lead to experimental difficulties in determining the flame structure. Except for optical measurement of NO^{4,6,8} and soot,^{5,9} few nonintrusive optical experimental data are available for this kind of adverse flame structure. In this work, we use Raman scattering measurement of temperature and major species concentrations to study the various opposed jet oxygen-enhanced flame structures. The oxygen concentration ranges from 21% to 100%. Planar opposed jet oxygen-enhanced methane flames are relatively thin and can be simplified into a

* Graduate Student, Student Member, AIAA

† Research Associate Prof., Senior Member, AIAA

‡ Prof. and Department Chair, Associate Fellow, AIAA

two-point boundary problem. The simulation of this kind flame structure with a complete chemical mechanism can be used to validate the kinetics. The radiation and soot only affect the flame temperature about 10 K with or without inclusion of the soot formation and radiation model.⁶ Therefore they will not be considered in the simulation. Flame structures are measured by the laser-based experiment and different chemical kinetic mechanisms for the high temperature flame are evaluated. The effect of oxygen enhancement on the flammability limit is also studied.

Experimental System and Flames Examined

Measurement of major species concentration and temperature are made along the centerline of an opposed jet burner using the nonintrusive Raman diagnostic system. The laser diagnostic system is similar to that described in Ref. 12. A schematic of the visible Raman system is shown in Fig. 1. A 532 nm Nd:YAG laser beam is stretched in time with a beam splitter and focused by a 0.3 m lens. A Stanford Research System DG535 pulse generator synchronizes the trigger signals in the system. The Raman light collecting system in Ref. 13 is modified by replacing the F/1.5 Cassegrain with a 75 mm diameter F/2 lens. The collimated light from this F/2 lens focused by a 75 mm diameter F/7.5 lens, passed through a ferroelectric shutter, a mechanical shutter, and an entrance slit to the 0.65 spectrometer. A mechanical shutter is used as an external shutter for the liquid nitrogen cooled CCD camera but it has relatively long exposure time (6 ms). A ferroelectric liquid crystal shutter is placed in front of the mechanical shutter to cut off flame luminosity into the spectrometer by its short exposure time (30 μ s). An orange Schott glass filter is placed in front of the entrance slit to block any stray 532 nm light. A separate IR filter (750 nm cutoff) is mounted at the entrance slit to eliminate the infrared radiation from the flame. A liquid-nitrogen-cooled, charge-coupled-device (LN/CCD) is used to obtain the Raman spectra. The LN/CCD camera has a 1024 x 1024 pixel chip, mounted to the back plane of the spectrometer. The chip is back-illuminated to give high quantum efficiency in the visible (~40%). The measuring sample volume is a cylinder (length is 4.7 mm and diameter is 0.2 mm). For the planar flame measurement, the 0.2 mm dimension is transverse to the concentration gradient. Thus, the 0.2 mm dimension is the spatial resolution of the system.

For the oxygen-enriched flame experiment, a safety system is designed that consists of a control system, a series of solenoid valves, check valves, and a high pressure purge nitrogen line. If the flame goes out, a solenoid valve automatically cuts off the fuel to ensure no flash back. The gas lines are cleaned for oxygen service. The opposed jet burner has been

modified from the design by Seshadri et al.¹⁴ and has been used extensively for hydrogen- and hydrocarbon-fueled diffusion flames and for hydrocarbon-fueled premixed flames. Also the opposed jet burner has been modified by inserting honeycomb metal “flow straighteners” into both nozzles. These inserts have 1/32-inch honeycomb cells that are 3/4 inch in length. The inserts provide a very uniform exit velocity profile for both nozzles, as verified by hot wire anemometry traverses in the nonreacting flow.

Numerical Simulations and Mechanisms

The diffusion flame formed by two axisymmetric opposed jets can be modeled by OPPDIF¹⁵ application software, which is part of CHEMKIN package. Detailed chemical kinetic mechanisms and transport data are used for the numerical predictions. GRI-Mech 3.0¹⁶ and Williams et al.¹⁷ chemical kinetic mechanisms are used for the oxygen-enhanced methane flames.

Results and Discussion

(1) Stretch rate effect on the structure of oxygen-enhanced flames

Stretch can affect the diffusion flame structure significantly. The flame thickness is decreased as the stretch rate is increased ($\delta \sim (D/k)^{1/2}$) due to the finite diffusion rate, D , as discussed by Sung et al.¹⁸ With increasing stretch rate, the chemical reaction time is shorter than the reactant residence time and incomplete reaction will cause the flame to extinguish. In order to see how oxygen enrichment and stretch affect the flame structure, the oxygen-enhanced flame structure at three stretch rates ($\kappa=60, 130$ and 168 s^{-1}) are shown in Figs. 2-4. Each flame has the same reactant concentration, that is, oxidizer jet is 30% O_2 -70% N_2 and fuel jet is 20% CH_4 -80% N_2 , but at different stretch rate. Fig. 2 shows the flame structure at stretch rate $\kappa=60 \text{ s}^{-1}$. It can be seen that major species (O_2 , CH_4 , H_2O) and temperature have a good agreement based on the comparison of experimental data and predictions that use the GRI-Mech 3.0 kinetic mechanism. There are differences between the measurements and the predictions. The predicted CO_2 is somewhat below the measurements and the measured oxygen leaks through the flame whereas the predicted O_2 is nearly zero at the flame front. The measured peak temperature is about 1883 K (± 16 K), the measured peak CO_2 is 5.6% ($\pm 0.2\%$), the measured peak H_2O is 13.1% ($\pm 0.3\%$). The flame thickness is 3.5 mm based on the full width at half maximum of the temperature profile. The error bars which are calculated based on shot noise are given for representative data. With the stretch rate rising to 130 s^{-1} , the flame structure is shown in Fig. 3. Again, temperature and species concentration have very good

agreement except for the differences in CO_2 and O_2 mentioned earlier. Even doubling the stretch rate κ , the peak temperature is almost unchanged (1850 K). The GRI-Mech 3.0 chemical kinetic mechanism works very well. Obviously the flame thickness (about 2 mm) decreases at this higher stretch rate. Continuing to increase stretch rate to the $\kappa=168 \text{ s}^{-1}$, the flame becomes thinner and flame structure is shown in Fig. 4. GRI-Mech 3.0 and Williams mechanism are used for numerical simulation for this flame. Identical results are obtained for both chemical kinetic mechanisms. Also the model-data comparison shows an excellent match between the experimental data and numerical results except for the deviations in O_2 and CO_2 mentioned before.

In order to show the effect of the stretch rate and O_2 concentration on the flame structure, the temperature profiles for $\kappa=60$ and 168 s^{-1} are shown in Fig. 5. At $\kappa=168 \text{ s}^{-1}$ and 30% O_2 , the temperature slightly drops and the flame zone (thickness) becomes narrower than the $\kappa=60 \text{ s}^{-1}$ condition. Further in order to identify the oxygen enhanced effect, maintaining the stretch rate at $\kappa=60 \text{ s}^{-1}$, the oxygen concentration is lowered to 23%. It is found that when oxygen concentration is close to 23%, the flame is near extinction for $\kappa=60 \text{ s}^{-1}$. From Fig. 5, there is 200 K drop when oxygen concentration changes from 30% to 23%. Also flame thickness becomes thicker. Further experiments indicate that there is no flame existing (extinction) when using air (21% O_2) as oxidizer at this stretch rate. The enriched oxygen “strengthens” the combustion because of a reduced amount of inert nitrogen in the reactant. The trend of peak NO_x concentration change with stretch rate is given in Fig. 6 for a constant oxidizer (30% O_2) and fuel (20% CH_4) stream concentration. There is a significant drop of calculated NO concentration (from 105 ppm to 70 ppm) when the stretch rate increases. This is because of reduced residence time and the slight temperature decrease. There is a similar trend for NO_2 where the concentration level of NO_2 is much lower than NO .

(2) Oxygen concentration effect on the structure of oxygen-enhanced flames

Oxygen is an important and common oxidizer. When oxygen-enriched mixtures are used as oxidizers instead of air, less nitrogen dilution in reactants will cause the flame temperature to increase significantly. This is one of the most important features for the oxygen-enriched flame. When the oxygen concentration changes from 31% to 100%, the detailed flame structures are shown in Fig. 2 and Fig. 7-10. Fig. 7 shows the detailed flame structure for the opposed jet flow where one jet has 41% O_2 -59% N_2 oxidizer stream and the other jet has a 20% CH_4 -80% N_2 fuel

stream. The reason for using diluted the fuel is that pure CH_4 produces significant interferences (i.e., laser induced fluorescence of PAH) for the laser-based Raman measurement. From Fig. 7, the calculated peak flame temperature is close to 2100 K. The measured species concentration profiles for O_2 , CH_4 , H_2O have a good agreement with simulation with GRI-Mech. 3.0 kinetic mechanism. In the flame zone, interference caused by C_2 emissions is much stronger than the 31% O_2 flame case. So the measured temperature slightly deviates from the simulated temperature. The measured CO_2 is also lower than the modeling results. Also, the measured O_2 leaks through the reaction zone while the predicted O_2 is nearly zero at that location.

The flame structure with 60% O_2 -40% N_2 oxidizer stream is shown in Fig. 8. With the increasing amount of O_2 , the peak temperature rises to 2300 K. The agreement between data and numerical results are still good for O_2 , CH_4 , and H_2O , but the LIF interference (from C_2 , soot and PAH) on the fuel stream side (near flame zone) cause unreliable experimental data (in shadowed region). Interference from the C_2 Swan band has been seen previously in Raman spectra in hydrocarbon flames¹⁹. Because this region is slightly off the region of peak flame temperature and it is only limited to a very small region, most of data are still reliable. The experimental CO_2 data still deviates from the simulated results and significant O_2 concentrations are measured at the flame zone. The profile of NO_x is given in Fig. 9. The concentration level of NO increases to 500 ppm when oxidizer varies from 30% O_2 (corresponding 105 ppm NO) to 60% O_2 . The oxygen-enhanced flame has this adverse potential to increase NO significantly for oxygen concentration less than 100%³. Fig. 10 shows the flame structure for 100% O_2 versus diluted CH_4 . For this extreme case, the flame temperature is 2550 K, a value much greater than the adiabatic temperature of CH_4 -air flames. The measured peak flame temperature (excluding the shadowed region) is 2416 K (± 63 K). The CO_2 and H_2O product concentrations are increased significantly. Strong emissions on the fuel stream side decreased the ratio of signal to noise and the experimental data is not reliable in this limited region (see shadowed region). Except for the thin interference zone, the measured species O_2 , H_2O , CH_4 , and temperature T have excellent agreement with model. For the stretch rate of $\kappa=60 \text{ s}^{-1}$, oxygen leakage exists in flame zone when oxygen concentration increases from 31% to 60%, but for pure oxygen case (100% O_2) shown in Fig. 10, almost all oxygen is consumed and no leakage is seen. The Williams mechanism has also been used for simulation giving nearly identical profiles for species and temperature to those obtained with the GRI-Mech 3.0 chemical kinetic mechanism.

Figure 11 summarizes the trend of CO₂, H₂O and temperature with oxygen concentration in the oxidizer. Generally all of these increase with O₂ concentration. For example, at the stretch rate $\kappa=60 \text{ s}^{-1}$, the calculated peak flame temperature jumps from 1694 K to 2503 K when O₂ concentration varies from 23% to 100%. The calculated CO₂ increases from 6.3% to 11.8% and calculated H₂O increases from 12% to 22% when the O₂ concentration changes from 23% to 100%. The experimental data for temperature and H₂O match with numerical results. However the measured CO₂ is always lower than the simulation results. Also in Fig. 11, the lowest measured oxygen concentration (extinction limit) is given (23%) at stretch rate $\kappa=60 \text{ s}^{-1}$ and a 20% CH₄-80% N₂ fuel stream. The predicted value of 22% oxygen is nearly the same. The calculated NO and NO₂ results with oxygen concentration change is given in Fig. 12. For these calculated flames, fuel stream is 20% CH₄ diluted by N₂. The increased temperature causes an increased formation of thermal NO_x as oxygen concentration is increased. The presence of N₂ in the fuel leads to formation at 100% oxygen.

(3) Near extinction limit flames

Oxygen-enriched oxidizer can enhance the combustion and should change the extinction limit. Fig. 13 shows the flame structure for another extreme case. It is 100% O₂ stream versus 8% CH₄-92% N₂ stream with the stretch rate $\kappa=60 \text{ s}^{-1}$. If fuel concentration is lower than 8%, the laboratory observed flame will go out (even though the numerical simulation predicts the lowest limit is 7% CH₄). From Fig. 13, it is found that peak flame temperature is only around 1600 K even though the oxidizer is 100% O₂. Model-data comparisons show all reactant, products and temperature match very well. Even the O₂ concentrations match well at the flame front. Similarly, when the oxidizer is 100% O₂, the peak flame temperatures (both experimental data and numerical results) are given in Fig. 14 with the CH₄ concentration varying from 7% to 20%. Just like varying oxidizer concentration, the fuel concentration changes the flame temperature significantly when 100% O₂ used as oxidizer. The measured and predicted extinction results are nearly the same except at 10% CH₄ where the temperature differs by 170 K.

In contrast to pure oxygen as the oxidizer, the flame structure with lowest fuel concentration is shown in Fig. 15 when the oxidizer is air (21% O₂ by volume). The lowest CH₄ concentration achieved in the experiment is 28% (volume) and simulation work shows the lowest limit is about 19% (volume). For this flame, temperature and species concentrations show a good agreement between the experimental data and the numerical results. However, the measured flame is

slightly weaker with a lower peak temperature (1681 K), CO₂ concentration and H₂O concentration than the predictions. The peak temperature trend with fuel concentration increasing is given in Fig. 16 when oxidizer is air and the stretch rate is $\kappa=60 \text{ s}^{-1}$. Compared to the results shown Fig. 14, the magnitude of temperature change is relatively small because the oxidizer is 21% O₂. Most striking is the large difference between the measured and calculated minimum for the methane concentration at extinction, 28% and 19%, respectively.

Conclusions

Planar oxygen-enhanced counterflow methane flames are investigated by optical diagnostics and numerical simulation. The effect of stretch and oxygen concentration in the oxidizer on the flame structure is studied in detail.

Oxygen concentration of reactants changes the flame temperature dramatically. At the same stretch rate $\kappa=60 \text{ s}^{-1}$, there is about 800 K difference in flame temperature when oxidizer varies from 23% O₂ to 100% O₂. Simulation with GRI-Mech 3.0 shows that model-data comparisons for reactants, products such as H₂O and temperature agree very well, but for CO₂, there is a consistent deviation for the oxygen-enriched flames. The measured CO₂ is consistently lower than the simulated results. This deviation becomes worse as oxygen concentration increased. The calculations show the oxygen is consumed at the flame front. However, in the experiments, oxygen leakage exists in flame zone at various oxygen-enhanced levels except for the pure oxygen case where the oxygen is completely consumed. Interference from the C₂ Swan band on fuel side disturbs the measurement only in very small vicinity so the overall flame structure can still be investigated by the Raman measurement.

The measured extinction limit for the minimum amount of fuel in the diluted fuel mixture is close to the calculated value when pure oxygen is used as an oxidizer, but when air is used, the measured extinction limit (28% CH₄ in N₂) for fuel mixture substantially deviates from the calculated result (19% CH₄ in N₂). Both the GRI-Mech 3.0 and Williams chemical kinetic mechanisms are used for numerical simulation. At low-level enrichment (30%) and high level oxygen-enrichment (100%), GRI-Mech 3.0 and Williams mechanisms give almost identical predictions.

Acknowledgements

This research work was partially supported by Gas Research Institute. Air Products provided most of the gases for oxygen-enhanced combustion experiment. The authors give special thanks for this support.

References

1. M. Pourkashanian, L. Yapp, and A. Williams, "The Use of Oxygen Enrichment in Combustion Technology," presented at Applied Energy Research Conference, Swansea, September, 1989.
2. C. E. Baukal, Jr, *Oxygen Enhanced Combustion*, CRC Press, Boca Raton, FL, 1999.
3. C. J. Sung, and C.K. Law, *Proc. Combust. Inst.* 27 (1998) 1411-1418.
4. S. V. Naik, and N. M. Laurendeau, *Combust. Flame* 129 (2002) 112-119.
5. A. Beltrame, P. Porshnev, W. Merchan-Merchan, A. Saveliev, A. Fridman, L. A. Kennedy, O. Petrova, S. Zhdanok, F. Amouri, O. Charon, *Combust. Flame.* 124 (1-2) (2001) 295-310.
6. S. V. Naik, N. M. Laurendeau, J. A. Cooke and M. D. Smooke, *Combust. Flame* 134 (2003) 425-431.
7. K. M. Leung, R. P. Lindstedt and W. P. Jones, *Combust. Flame*, 87 (1991) 289-305.
8. S. V. Naik and N. M. Laurendeau, *Combust. Sci. and Tech.*, 174 (2002) 1-21.
9. U. Vandsburger, I. Kennedy and I. Glassman, *Combust. Sci. and Tech.*, 39 (1984) 263-285.
10. O. Charon, D. Jouvaud, and B. Genies, *Combust. Sci. and Tech.* 93 (1993) 211-222.
11. W. Qin, J-Y. Ren, F. N. Egolfopoulos, S. Wu, H. Zhang, and T. T. Tsotsis, *Proc. Combust. Inst.* 28 (2000) 1825-1831.
12. Z. Cheng, J. A. Wehrmeyer, and R. W. Pitz, 38th AIAA/ASME/SAE/ASEE Joint Propulsion Conference AIAA 2002-4021, Indianapolis, IN, 2002.
13. J. A. Wehrmeyer, Z. Cheng, D. M. Mosbacher, R. W. Pitz, and R. Osborne, *Combust. Flame* 128 (3) (2002) 232-241.
14. K. Seshadri, I. Puri, and N. Peters, *Combust. Flame*, 61 (3) (1985) 237-249.
15. R. J. Kee, F. M. Rupey, J. A. Miller, M. E. Coltrin, J. F. Grcar, E. Meeks, H. K. Moffat, A. E. Lutz, G. Dixon-Lewis, M. D. Smooke, J. Warnatz, G. H. Evans, R. S. Larson, R. E. Mitchell, L. R. Petzold, W. C. Reynolds, M. Caracotsios, W. E. Stewart, and P. Glarorg, C. Wang., O. Adigum, W. G. Houf, C. P. Chou, and S. F. Miller, Chemkin Collection, Release 3.7, Reaction Design, Inc., San Diego, CA, 2002.
16. G.P. Smith, D.M. Golden, M. Frenklach, N. W. Moriarty, B. Eiteneer, M. Goldenberg, C. T. Bowman, R. K. Hanson, S. Song, W. C. Jr. Gardiner, V. V. Lissianski, and Z. Qin, <http://www.me.berkeley.edu/gri-mech/>.
17. <http://maeweb.ucsd.edu/~combustion/cermech>.
18. C. J. Sung, J. B. Liu, and C. K. Law, *Combust. Flame*, 102 (1995) 481-492.
19. R. S. Barlow, C. D. Carter, and R. W. Pitz, "Multiscalar Diagnostics in Turbulent Flames" in:

Applied Combustion Diagnostics, K. Kohse-Höinghaus and J.B. Jeffries, eds. Taylor and Francis, New York, 2002.

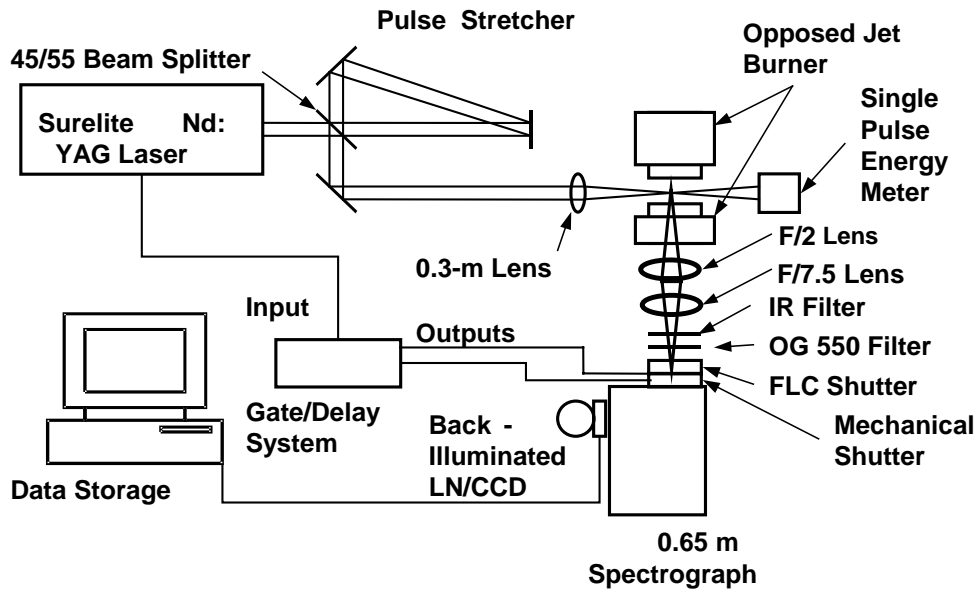


Fig. 1. Visible Raman system schematic.

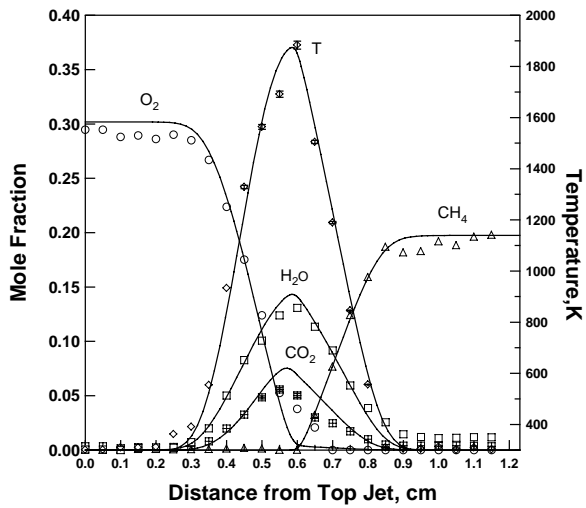


Fig. 2. Experimental and numerically-predicted species and temperature profiles for an oxygen-enriched diffusion flame: 30% O₂-70% N₂ vs. 20% CH₄-80% N₂, $\kappa=60 \text{ s}^{-1}$. Numerical simulation using GRI-Mech 3.0.

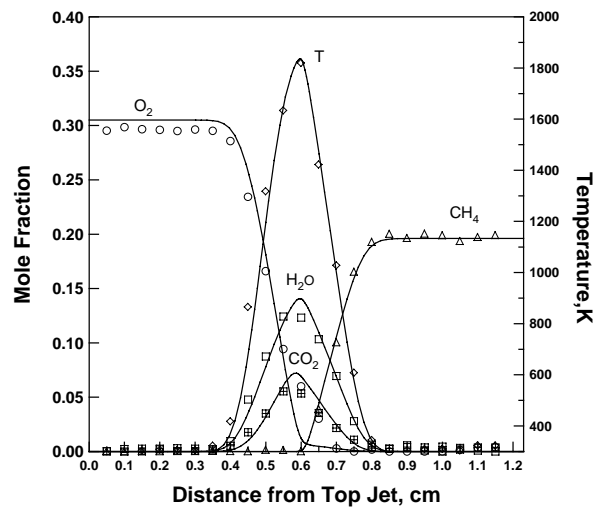


Fig. 3. Experimental and numerically-predicted species and temperature profiles for an oxygen-enriched diffusion flame: 31% O₂-69% N₂ vs. 20% CH₄-80% N₂, $\kappa=130 \text{ s}^{-1}$. Numerical simulation using GRI-Mech 3.0.

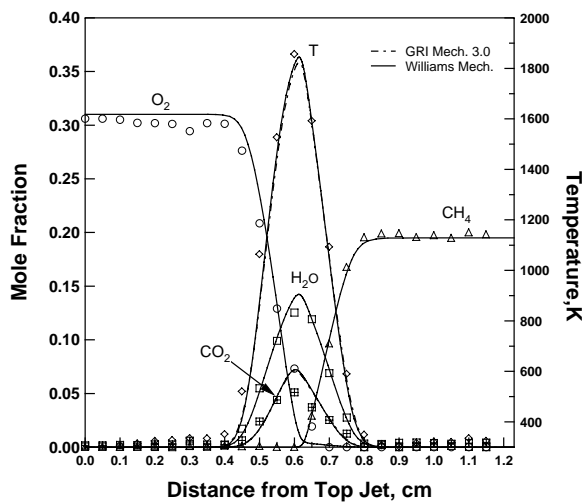


Fig. 4. Experimental and numerically-predicted species and temperature profiles for an oxygen-enriched diffusion flame: 31% O₂-69% N₂ vs. 20% CH₄-80% N₂, $\kappa=168 \text{ s}^{-1}$. Numerical simulation using GRI-Mech 3.0 and Williams mechanisms.

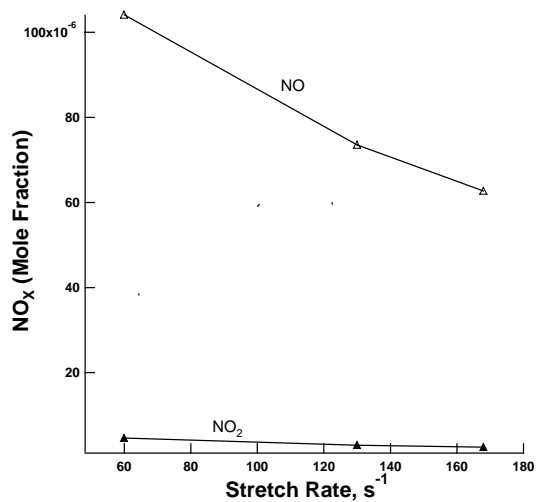


Fig. 6. Stretch rate effect on the numerically predicted NO_x. Flames are 30% O₂ vs. 20% CH₄-80% N₂. Numerical simulation using GRI-Mech 3.0.

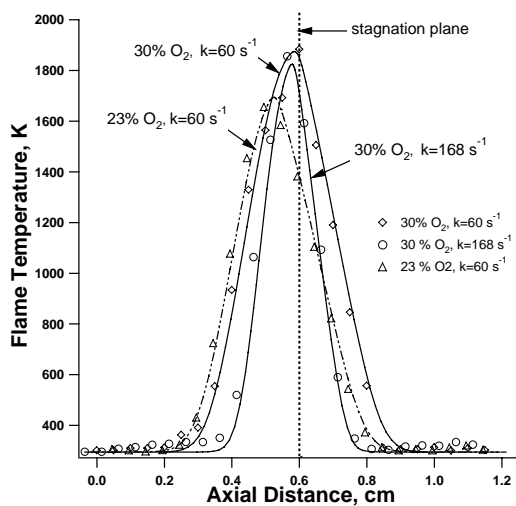


Fig. 5. Stretch effect and oxygen concentration effect on temperature profiles.

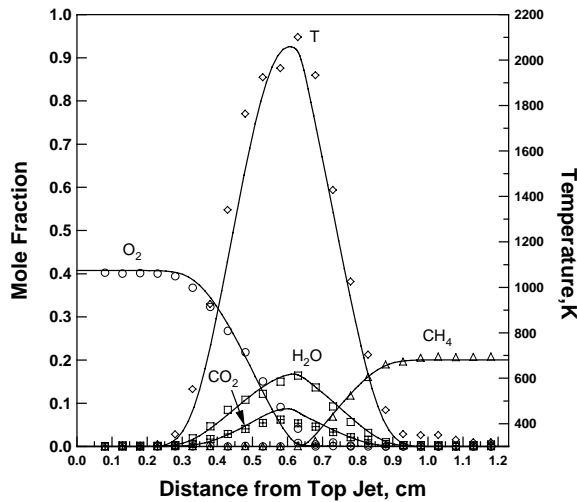


Fig. 7. Experimental and numerically-predicted species and temperature profiles for an oxygen-enriched diffusion flame: 41% O₂-59% N₂ vs. 20% CH₄-80% N₂, $\kappa=60 \text{ s}^{-1}$. Numerical simulation using GRI-Mech 3.0.

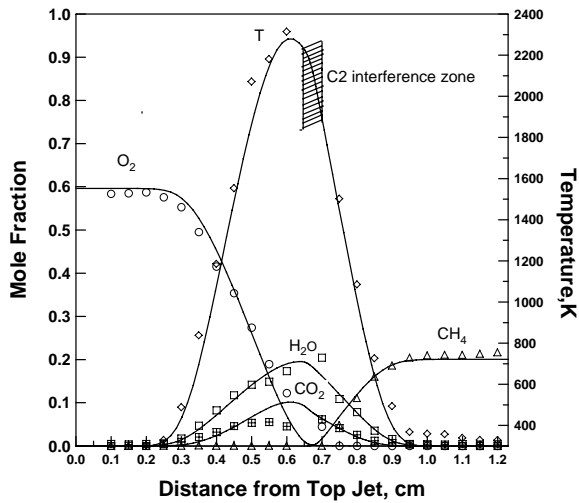


Fig. 8. Experimental and numerically-predicted species and temperature profiles for an oxygen-enriched diffusion flame: 60% O₂-40% N₂ vs. 20% CH₄-80% N₂, $\kappa=60 \text{ s}^{-1}$. Numerical simulation using GRI-Mech 3.0.

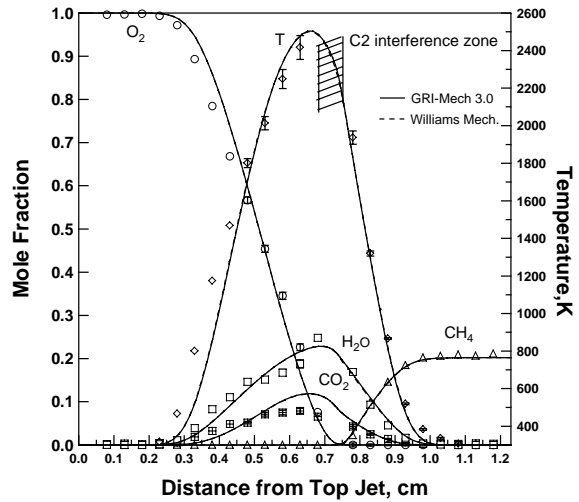


Fig. 10. Experimental and numerically-predicted species and temperature profiles for an oxygen-enriched diffusion flame: 100% O₂ vs. 20% CH₄-80% N₂, $\kappa=60 \text{ s}^{-1}$. Numerical simulation using GRI-Mech 3.0 and Williams mechanism.

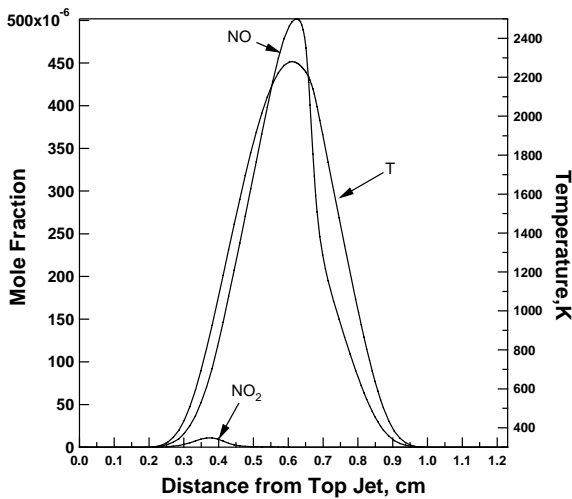


Fig. 9. Numerically-predicted NO_x and temperature profiles for a diffusion flame: 60% O₂-40% N₂ vs. 20% CH₄-80% N₂, $\kappa=60 \text{ s}^{-1}$. Numerical simulation using GRI-Mech 3.0.

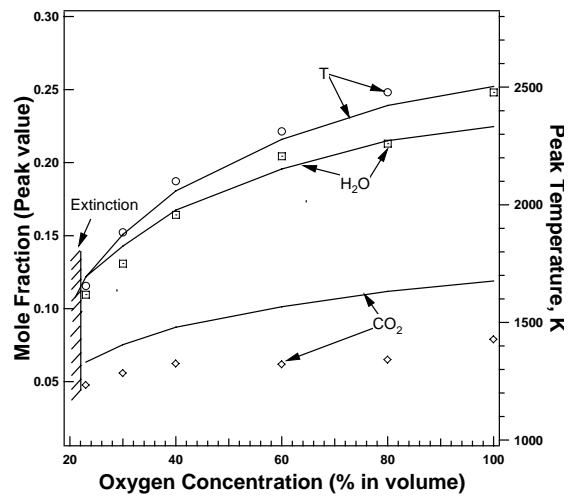


Fig. 11. Oxygen concentration effect on temperature, H₂O and CO₂ profiles. Numerical simulation using GRI-Mech 3.0. The stretch rate is 60 s⁻¹ and the fuel stream is 20% CH₄-80% N₂.

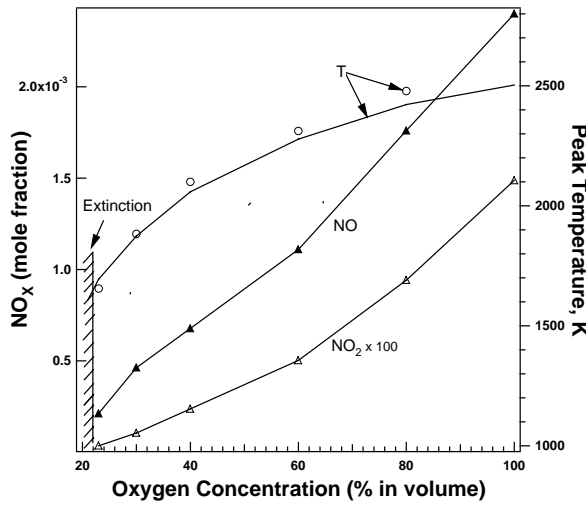


Fig. 12. Oxygen concentration effect on numerically predicted NOx. Experimental and numerically predicted temperature shown for reference from Fig. 11. Numerical simulation using GRI-Mech 3.0.

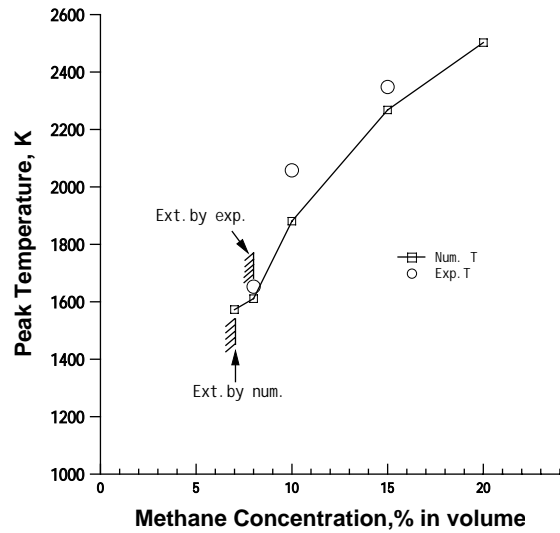


Fig. 14. CH₄ concentration effect on temperature profiles when oxidizer is pure O₂. Stretch rate is 60 s⁻¹.

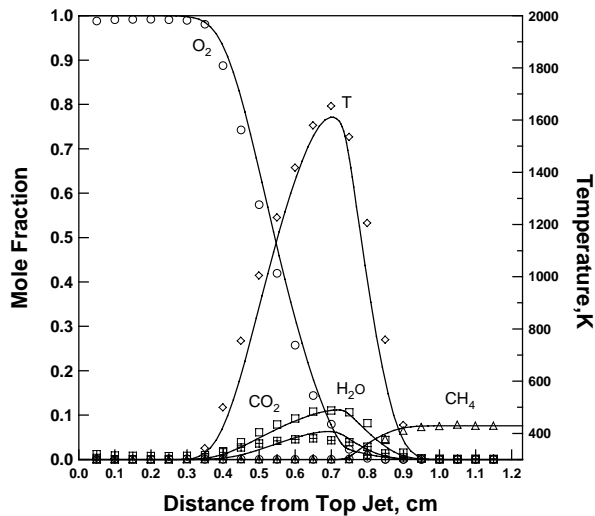


Fig. 13. Experimental and numerically-predicted species and temperature profiles for an oxygen-enriched diffusion flame: 100% O₂ vs. 8% CH₄-92% N₂, $\kappa=60$ s⁻¹. Numerical simulation using GRI-Mech 3.0.

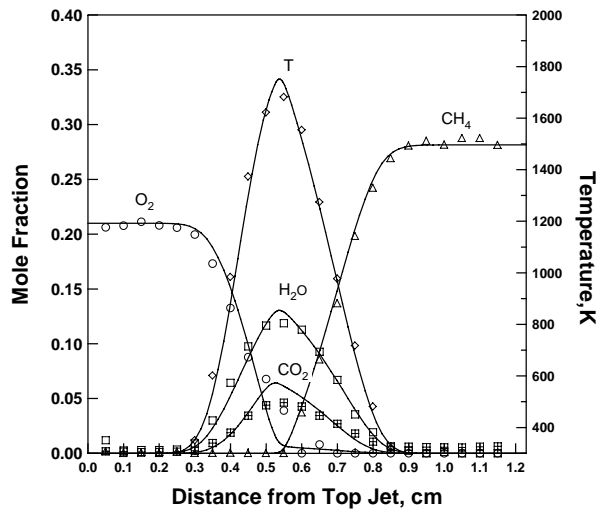


Fig. 15. Experimental and numerically-predicted species and temperature profiles for a near extinction flame diffusion flame: 28% CH₄-72% N₂ vs. air, $\kappa=60$ s⁻¹. Numerical simulation using GRI-Mech 3.0.

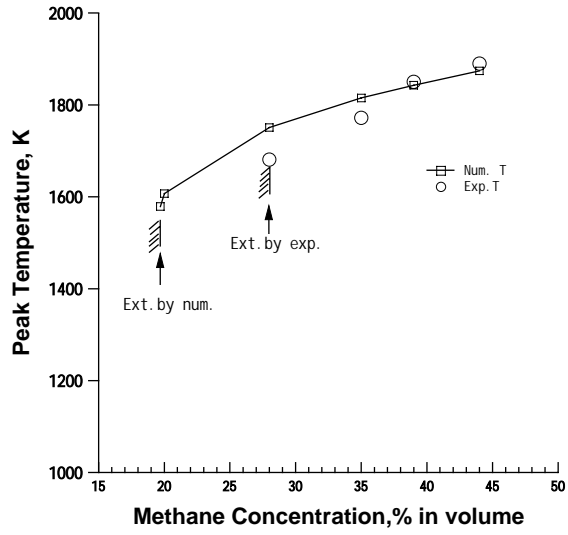


Fig. 16. CH₄ concentration effect on temperature profiles when oxidizer is air. Stretch rate is 60 s⁻¹.